Published in final edited form as:
Neuroimage. 2009 August ; 47(Suppl 2): T27–T35. doi:10.1016/j.neuroimage.2008.11.012.

Real-time MR imaging of adeno-associated viral vector delivery to the primate brain

Massimo S. Fiandaca[a], **Vanja Varenika**[a], **Jamie Eberling**[a,b], **Tracy McKnight**[c], **John Bringas**[a], **Phillip Pivirotto**[a], **Janine Beyer**[a], **Piotr Hadaczek**[a], **William Bowers**[d], **John Park**[e], **Howard Federoff**[f], **John Forsayeth**[a], and **Krystof S. Bankiewicz**[a,*]

[a]Department of Neurological Surgery, University of California San Francisco, 1855 Folsom Street, Room 226, San Francisco, CA 94103, USA

[b]Center For Functional Imaging, Lawrence Berkeley National Laboratory, Berkeley, CA, USA

[c]Department of Radiology, University of California San Francisco, San Francisco, CA, USA

[d]University of Rochester, Rochester, NY, USA

[e]Hematology/Oncology Department, University of California San Francisco, San Francisco, CA, USA

[f]Georgetown University, Washington, D.C., USA

Abstract

We are developing a method for real-time magnetic resonance imaging (MRI) visualization of convection-enhanced delivery (CED) of adeno-associated viral vectors (AAV) to the primate brain. By including gadolinium-loaded liposomes (GDL) with AAV, we can track the convective movement of viral particles by continuous monitoring of distribution of surrogate GDL. In order to validate this approach, we infused two AAV (AAV1-GFP and AAV2-hAADC) into three different regions of non-human primate brain (corona radiata, putamen, and thalamus). The procedure was tolerated well by all three animals in the study. The distribution of GFP determined by immunohistochemistry in both brain regions correlated closely with distribution of GDL determined by MRI. Co-distribution was weaker with AAV2-hAADC, although *in vivo* PET scanning with FMT for AADC activity correlated well with immunohistochemistry of AADC. Although this is a relatively small study, it appears that AAV1 correlates better with MRI-monitored delivery than does AAV2. It seems likely that the difference in distribution may be due to differences in tissue specificity of the two serotypes.

Keywords

Adeno-associated virus; Gadolinium; Liposomes; Thalamus; Putamen; Corona radiata

Introduction

Convection-enhanced delivery (CED) uses fluid pressure at the tip of the delivery cannula and bulk flow to propagate substances within the extracellular fluid spaces (Bobo et al., 1994). Our understanding of CED distribution has been further enhanced by elucidation of the physiologic effects of the local pulsatile vasculature (Hadaczek et al., 2006b), the complexities of the extracellular matrix (Hamilton et al., 2001; Neeves et al., 2007; Nguyen et al., 2001), and the

*Corresponding author. Fax: +1 415 514 2864. Krystof.Bankiewicz@ucsf.edu (K.S. Bankiewicz).

biophysical properties of the extracellular space volume fraction (Sykova, 2004). With the increasing use of CED in clinical neurosurgery (Kunwar et al., 2007; Lonser et al., 2007), investigators have sought to visualize the delivery of therapeutics intra-operatively. CED visualization with the aid of novel contrast materials co-infused with therapeutic agents has recently been investigated in rodents (Saito et al., 2004), non-human primates (Lonser et al., 2002; Murad et al., 2007; Saito et al., 2005) and humans (Lonser et al., 2007; Sampson et al., 2007). Real-time convective delivery (RCD) utilizes MRI to visualize the CED process with the aid of Gadolinium-loaded liposomes (GDL) to co-distribute with the therapeutic being delivered.

Adeno-associated viral vectors (AAV) contain single-stranded DNA genomes and are members of the nonpathogenic parvovirus family. They are capable of delivering gene constructs of almost 5 kb (Baekelandt et al., 2000; Grieger and Samulski, 2005). Since 1982, when the first infectious AAV2 clone was established (Samulski et al., 1982), over 20 clinical gene therapy trials have been conducted with AAV2 vectors for the treatment of a variety of diseases and have included several hundred patients (Carter, 2005). True AAV serotypes include AAV1-5 and AAV7-9, whereas variants AAV6, 10, and 11 do not fit the serotype definition, sharing serology with others or otherwise poorly characterized (Wu et al., 2006). Recent reviews (Gao et al., 2006; Grimm and Kay, 2003) have improved our understanding of the AAV serotypes with respect to their isolation, serology, classification and potential application to gene therapy. Optimal viral vector delivery into the brain, however, continues to be a challenge despite an advanced understanding of the mechanisms involved. AAV cellular tropism in the brain appears to be related to viral capsid composition, rather than the enclosed vector genome (Vite et al., 2003), with AAV1 tending to target both glia and neurons and AAV2 being much more neuron-specific. AAV2 has been selected as the viral vector of choice in three recent human intra-cerebral gene therapy trials for Parkinson's disease (PD) (Fiandaca et al., 2008). Our group has demonstrated that CED is an efficient method for the distribution of the AAV vector in the brains of rats (Hadaczek et al., 2006b; Sanchez-Pernaute et al., 2001), monkeys (Hadaczek et al., 2006a; Sanftner et al., 2005), and humans (Eberling et al., 2008). Parameters required for optimal delivery of AAV vector, such as infusion volume (Vi), rate of infusion, and optimal cannula type and placement, had to be defined experimentally (Chen et al., 1999; Krauze et al., 2005b; Szerlip et al., 2007) to improve delivery efficiency, while attempting to limit the spread of vector into regions outside the target volume, including the CSF. Despite optimization of these parameters, and use of RCD, inadvertent leakage of therapeutic agents during CED continues to be an issue (Varenika et al., 2008).We continue to refine our AAV delivery platform and the current study was designed to investigate the correlation between (1) RCD of GDL delivered with AAV into the parkinsonian NHP brain, (2) post-CED FMT-PET, and (3) post-mortem immunohistochemistry (IHC) of the infused brain regions. The sites of CED infusion included the corona radiata, striatum, and thalamus. Our MRI contrast agent was GDL and was delivered with either AAV1-GFP or AAV2-hAADC.

Materials and methods

Experimental subjects

Adult male non-human primates (*Macaca mulata*, *n*=3, 3–10 kg), abbreviated NHP, were individually housed in stainless steel cages. Each animal room was maintained on a 12-hour light/dark cycle, and room temperature ranged between 64 °F and 84 °F. Purina Primate Diet was provided on a daily basis in amounts appropriate for the size and age of the animals. This dietwas supplemented with fruit or vegetables daily. Also, small bits of fruit, cereal, or other treats were provided as part of the environmental enrichment program. Tap water was freely available to each animal through an automatic watering device or an attached water bottle.

Parkinsonism in NHP (*Macaca mulatta*) was induced by administration of 2–4 mg MPTP into the internal carotid artery as previously described (Bankiewicz et al., 1986). MPTP-treated animals used for this study were not suitable for functional studies due to unstable PD signs. Animal protocols were reviewed and approved by the Institutional Animal Care and Use Committees at the University of California San Francisco (San Francisco, CA).

Liposomal preparation

Separate liposomes were prepared for detection by MRI and by histological examination as previously described (Krauze et al., 2005a; Mamot et al., 2003, 2004; Saito et al., 2004, 2005). Liposomes that contained the MRI contrast agent were composed of 1,2-dioleoyl-snglycero-3-phosphocholine (DOPC)/cholesterol/1,2-distearoyl-sn-glycero-3-[methoxy (polyethylene glycol)-2000 (PEG-DSG) with a molar ratio of 3:2:0.3. DOPC was purchased from Avanti Polar Lipids (Alabaster, AL), PEG-DSG was purchased from NOF Corporation (Tokyo, Japan), and cholesterol was purchased from Calbiochem (San Diego, CA). The lipids were dissolved in chloroform/methanol (90:10, vol/vol), and then the solvent was removed by rotary evaporation, resulting in a thin lipid film. The lipid film was dissolved in ethanol and heated to 60 °C. A commercial United States Pharmacopoeia solution of 0.5 M Gadoteridol (10-(2-hydroxy-propyl)-1,4,7,10-tetraazacyclododecane-1,4,7-triacetic acid (Prohance; Bracco Diagnostics, Princeton, NJ) was heated to 60 °C and injected rapidly into the ethanol/lipid solution. Unilamellar liposomes were formed by extrusion (Lipex; Northern Lipids, Vancouver, Canada) with 15 passes through double-stacked polycarbonate membranes (What man Nucleopore, Clifton, NJ) with a pore size of 100 nm, resulting in a liposome diameter of 124±24.4 nm as determined by quasi-elastic light scattering (N4Plus particle size analyzer, Beckman Coulter, Fullerton, LA). Unencapsulated Gadoteridol was removed with a Sephadex G-75 (Sigma, St. Louis, MO) size-exclusion column eluted with HEPES-buffered saline (5 mM HEPES, 135 mM NaCl, pH 6.5, adjusted with NaOH).

Liposome infusion in NHP

All three animals received a baseline MRI scan, and underwent neurosurgical procedures to position an MRI-compatible guide-cannula within specific regions of the brain (e.g. putamen, corona radiata, and thalamus). Each guide-cannula was specifically customized for the procedure and stereotactically guided to reach its target through a burr-hole created in the skull. Each guide-cannula was secured to the skull with dental acrylic, and the tops of the guide-cannula assemblies were capped with stylet screws for simple access during the infusion procedure. Animals recovered for at least 2 weeks before initiation of liposome infusions. During each liposome-enhanced infusion procedure, the animal was anesthetized with isoflurane, the head was placed in an MRI-compatible stereotactic frame and a baseline MRI scan was performed. Vital signs, such as heart rate and pO_2, were monitored throughout the procedure. Infusions were performed according to previously established CED techniques for non-human primates (Bankiewicz et al., 2000; Krauze et al., 2005b). Briefly, the infusion system consisted of a fused-silica needle cannula that was connected to a loading line (containing liposomes) and an oil-infusion line. A 1-ml syringe (filled with oil), mounted onto a micro-infusion pump (BeeHive; Bioanalytical Systems, West Lafayette, IN), regulated the flow of fluid through the system. Based on MRI coordinates, the cannula was mounted onto a stereotactic holder, and manually guided to the targeted regions of the brain through the previously placed guide-cannula. The length of each infusion cannula was measured to ensure that the distal tip extended approximately 3 to 4 mm beyond the length of the respective guide. This created a stepped design at the tip of the cannula to maximize fluid distribution during CED procedures. After secure placement of the needle cannula, the animal's head was repositioned in the MRI gantry and CED procedures were initiated while MRI data was being continuously acquired. Infusion volumes into each targeted site ranged between 40 and 70 µl. An initial infusion rate of 0.2 µl/min was applied and increased sequentially to 0.5, 0.8, 1.0,

1.5 μl/min, and finally to 2.0 μl/min at 10-min intervals. The approximate concentration of liposomes injected corresponded to a formulated concentration of 10 mM phospholipids and 5 mM Gadoteridol. Approximately 15 min after infusion, the cannula was withdrawn from the brain. The animals were euthanized 8 weeks after the infusion procedures, and the brains were harvested according to the procedure described below.

Quantification of liposome-entrapped Gadoteridol (GDL) by MRI

The concentration of Gadoteridol entrapped in the liposomes was determined from nuclear MR relaxivity measurements. The relationship between the change in the intrinsic relaxation rate imposed by a paramagnetic agent (ΔR), also known as "T1 shortening," and the concentration of the agent is defined by the equation: ΔR=r1[agent], in which r1=relaxivity of the paramagnetic agent and ΔR=(1 /T1observed−1/T1intrinsic). The relaxivity of Gadoteridol had been empirically derived previously on the same system, a 2-Tesla Brucker Omega scanner (Brucker Medical, Karlsruhe, Germany), and had a value of 4.07 mM^{-1} s^{-1}. The concentration of the encapsulated Gadoteridol was then calculated with the following equation: [Gadoteridol] =[(1 /T1wGado)−(1 /T1w/oGado)]/4.07.

Magnetic resonance imaging acquisition

Animals underwent MR imaging before surgery to visualize anatomical landmarks and to generate stereotactic coordinates of the target implant sites for each animal. During the baseline scanning procedure, each animal was sedated with a mixture of intramuscular (I.M.) ketamine (Ketaset, 7 mg/kg) and xylazine (Rompun, 3 mg/kg, I.M.). The head was placed in an MRI-compatible stereotactic frame, ear-bar and eye-bar measurements were recorded, and an intravenous line was established. Sixty coronal images (1 mm) and 15 sagittal images (3 mm) were taken with a GE Signa (GE Medical Systems, Milwaukee, WI) 1.5 Tesla machine. Targeted regions of the brain were visualized with coronal T1-weighted spoiled gradient echo images. The following imaging parameters were applied during the procedure: TR/TE/flip angle=40 ms/6 ms/30°, 2 NEX, matrix=256×256 or 384×256, FOV=18–22 cm, slice thickness=1.0 mm. These parameters showed voxel sizes that ranged from 1.2×10^{-4} cm^3 to 1.2×10^{-3} cm^3. Rostrocaudal and mediolateral distribution of a targeted structure (e.g., putamen) were determined from the coronal MR images. Surgical coordinates were generated from magnified coronal images of the corona radiata, putamen, and thalamus.

Positron emission tomography

Animals received PET scans at baseline (pre-surgery), and approximately 6 weeks after intracranial AAV2-hAADC administration. Imaging techniques were similar to those previously described (Bankiewicz et al., 2000). PET studies were performed on a Siemens ECAT EXACT HR PET scanner in 3D acquisition mode. The tracer, 6-[^{18}F] fluoro-L-m-tyrosine (FMT), was synthesized by a modification of a previously described procedure (Namavari et al.,1993). Monkeys were anesthetized with an intramuscular injection of ketamine (15 mg/kg), intubated and anesthetized with isoflurane. All animals were pretreated with an intravenous injection of benserazide (2 mg/kg), a peripheral decarboxylase inhibitor, 30 min before imaging. The animals were placed in a stereotactic frame and positioned in the PET scanner. Images were obtained in the coronal plane. Prior to the emission scan a 10-min transmission scan was obtained for attenuation correction. Subsequently, approximately 3–5 mCi of FMT was injected as a bolus in an antecubital vein and a 90-min dynamic acquisition sequence was acquired.

Data were reconstructed by an ordered subset expectation maximization (OSEM) algorithm with weighted attenuation, an image size of 256×256, and 6 iterations with 16 subsets. A Gaussian filter with 6-mm FWHM and a scatter correction was applied. PET data were quantified with a multiple time graphical analysis ("Patlak plot") by means of the time activity-

curve for a region, in the case of FMT-PET the cerebellum, in which the tracer is non-specifically bound as the input function. This approach has the obvious advantage of not requiring arterial blood sampling. Rather than the term K_i, FMT uptake in a region of interest (ROI) will be referred to as K_i^c to denote that the cerebellum was used as the reference region. We calculated K_i^c on a voxel-wise basis in order to construct a K_i^c image in native space for each monkey at each time point.

Histological procedures

Our histological protocol has been previously published (Bankiewicz et al., 2000). In brief, animals were deeply anesthetized with sodium pentobarbital (25 mg/kg i.v.) and euthanized approximately 8 weeks after AAV administration. The body was cardiac perfused with Zamboni's fixative (Stefanini et al., 1967), the brain harvested and coronally sliced with a brain matrix. The formalin-fixed brain slices were cut into 40-μm coronal sections in a cryostat. Sections were collected in series starting at the level of the rostral tip of the caudate nucleus all the way caudally to the level of the substantia nigra. Sections were processed for immunohistochemistry (IHC) and H&E staining. Serial sections were stained for aromatic human Lamino acid decarboxylase (hAADC) and green fluorescence protein (GFP). Every 10th section was washed in phosphate buffered saline (PBS) and incubated in 3% H_2O_2 for 20 min to block the endogenous peroxidase activity. After washing in PBS, the sections were incubated in blocking solution (10% normal horse serum for TH or 10% normal goat serum for AADC and B-gal and 0.1% Triton-X 100 in PBS) for 30 min, followed by incubation in primary antibody solution-AADC (rabbit polyclonal, Chemicon, 1:2000) or GFP (rabbit polyclonal, Chemicon, 1:500) for 24 h. The sections were then incubated for 1 h in anti-rabbit IgG secondary antibody for AADC and GFP (Vector Labs, 1:300). The antibody binding was visualized with streptavidin horseradish peroxidase (Vector Labs, 1:300) and DAB chromagen with nickel (Vector Labs). Sections were then examined under a light microscope.

Volume quantification from histology

The volumetric analysis of AAV1-GFP and AAV2-hAADC expression was performed with a Zeiss light microscope. GFP- and AADC-positive areas were identified at low magnification. Positively transduced cells were confirmed under high magnification. The exact topographic locations of these areas were determined with printed images from a Rhesus monkey brain atlas (Paxinos and Watson, 1982). Areas staining positive on primate histology were manually transferred to corresponding primate CNS MRI. This was accomplished by delineating positive areas on corresponding baseline MR images with BrainLAB software (BrainLAB, Heimstetten, Germany). This software allows for 3D re-construction of expression on MRI and computation of the distribution volume (Vd).

Volume quantification from MR images

The volume of liposomal distribution within each infused brain region was quantified with BrainLAB software. *MR* Images acquired during the infusion procedure were correlated with volume of infusion (Vi) at each series started during an infusion procedure. The software reads all data specifications from *MR* images. After the pixel threshold value for liposomal signal is defined, the software calculates the signal above a defined threshold value, and establishes the Vd from primate brain. This allows Vd to be determined at any given time-point and can be reconstructed in a three-dimensional image.

Production of AAV

Recombinant AAV1-GFP was produced in insect cells with a recombinant baculovirus (Urabe et al., 2002). AAV2-hAADC (human Aromatic L-amino Acid Decarboxylase) was constructed by a triple transfection technique (Matsushita et al., 1998; Wright et al., 2003). Both vectors

underwent CsCl gradient centrifugation to remove empty capsids. AAV1-GFP and AAV2-hAADC were obtained at a stock concentration of 2.9×10^{12} and 7.0×10^{12} vector genomes/ml in phosphate-buffered saline (pH 7.4) and Pluronic F-68 (0.001% v/v).

Results

We obtained real-time MR imaging data of the co-distribution of AAV gene therapy with GDL from all three NHP. The sites of CED and the infused materials are schematically represented and summarized for each subject (NHP1, NHP2, and NHP3) (Fig. 1). The thalamic infusions contained 40−70 μl of AAV1-GFP/GDL, whereas 60–70 μl of AAV2-hAADC/GDL was infused into the putamen, and 50–70 μl of AAV1-GFP/GDL was delivered into the corona radiata. Each of our subjects had unilateral corona radiata and thalamic gene therapy. Two animals received bilateral putaminal gene therapy, whereas the third received only unilateral infusion. All three NHP tolerated the stereotactic RCD procedure without noticeable post-operative deficits. Animal behavior was not altered significantly by the CED gene therapy and GDL co-infusion during the 8 weeks after AAV delivery. In addition, based on considerable experience with striatal infusions of NHP's both bilaterally (Forsayeth et al., 2006) and unilaterally (Bankiewicz et al., 2006) with AAV2-hAADC, we have never noted any difference in any parameters based on unilateral vs bilateral infusions.

Magnetic resonance imaging (MRI)

Representative MRI images of the three infusion sites (Fig. 2) show dispersal of GDL in a manner typical of previous real-time MRI visualizations of CED in the NHP brain (Krauze et al., 2006,2008). In both the putaminal and thalamic convections, visualized GDL on MRI tended to extend beyond the limits of the anatomic nucleus and into surrounding white matter. Similarly, CED within the corona radiata extended primarily into the white matter but also spread into the adjacent basal ganglia. Despite the use of a reflux-resistant cannula and relatively low infusion rates, some reflux along the cannula tract or dispersal of GDL into the subarachnoid spaces was noted (Fig. 2B), as previously reported (Varenika et al., 2008).

PET imaging

In the 3 hemi-parkinsonian NHP's, FMT-PET data was obtained pre-operatively and 6 weeks after AADC gene therapy (Fig. 3). The transduced putamen showed a significant increase in FMT-PET signal compared to baseline. This is similar to what has been seen in NHP previously (Bankiewicz et al., 2000) and in human subjects with a comparable transgene (Eberling et al., 2008).

Immunohistochemistry

Histological analysis of the NHP brains allowed visualization of GFP (Fig. 4 and Fig. 5) and AADC (Fig. 6) staining with immunohistochemistry (IHC) of coronal sections. GFP staining was noted within both gray and white matter structures, but AADC staining was limited to gray matter. IHC for AADC was correlated with post-infusion FMT-PET images. Similar to the MRI correlation with PET (Fig. 3), there was close overlap of the transduced AADC neuronal regions and the FMT-PET signal (data not shown).

Comparative analysis of MRI and histology

Vd measurements were obtained for GDL from MRI images and IHC staining of either GFP or AADC on serial brain sections. The Vd for GDL and the comparable IHC was obtained for each different RCD in the three NHP. The Vd of GDL and GFP expression were nearly identical, but this was not the case with GDL and AADC (Fig. 7A). As noted in the qualitative assessments described above, GDL imaging and GFP staining overlapped within both gray

and white matter structures. Although GDL, AAV1-GFP, and AAV2-hAADC spread similarly within both gray and white matter, IHC confirmed that AAV2-hAADC did not transduce cells within white matter regions (Fig. 6). This accounted for the diminished similarity between the Vd of GDL and AAV2-hAADC transfection. When only the gray matter Vd of GDL in cases of AAV2-hAADC RCD is considered, however, there is little difference between the two measures (Fig. 7B), similar to that seen with GDL and AAV1-GFP.

Discussion

Our study underlines the importance of the viral serotype used for gene therapy, even when technology such as RCD provides an additional level of confidence in the intra-operative distribution of therapeutics. Although this is a relatively small study in which only three animals were used, there is an apparent discrepancy between the MR imaging of GDL and histological localization of the hAADC transgene when AAV2 is used as the viral carrier. Extension of the GDL into the white matter does not correlate with AADC localization in that region, as determined by IHC, since AAV2 does not have a significant affinity for non-neuronal cells. There is a closer correlation between AADC IHC and FMT-PET scanning, showing close overlap between histological sections co-registered with PET images. In similar RCD scenarios AAV1-GFP/GDL correlated well with IHC staining for GFP in both gray and white matter, since AAV1 allows transfection in both of these regions. The ability to predict the distribution of AAV1 transduction with MRI of GDL, therefore, seems accurate.

RCD with GDL and other equivalent markers may provide the accuracy of delivery and reproducibility necessary for treating physicians to gain confidence in this delivery platform. The applicability of this platform to a variety of neurological diseases makes it particularly relevant to the neurosurgeon and clinical neuroscientist as the field moves towards direct drug delivery to the central nervous system (CNS). Although the GDL contrast agent has not shown any tissue toxicity in early NHP studies (Krauze et al., 2008), further investigation of this and other MRI contrast agents is warranted before human trials. This is especially important in light of recent FDA warnings about gadolinium-related imaging agents concerning potential toxicity and death secondary to nephrogenic systemic fibrosis (NSF) in patients with severe renal insufficiency receiving these compounds[1]. In this regard, one of the most relevant mechanistic problems in the treatment of PD with either gene therapy or growth factor protein infusion is accurate determination of the extent of distribution of the delivered vector or protein within the brain parenchyma. Visualization of the infusate in post-operative MRI studies, without a contrast agent, has been problematic in our early experiences with AAV2-hAADC gene therapy in PD patients (K.S.B, unpublished data). Without this imaging capability, treating physicians must predict Vd based on NHP studies and comparative anatomical ratios between NHP and human (Yin et al., in press). Thus, a direct visualization of the CED process used to deliver viral vectors or macromolecules should be more accurate and less prone to interpretive error. RCD also confirms the targeting and allows for optimization prior to or during the CED procedure, as we have done in animal studies (Varenika et al., 2008).

Since the GDL contrast agent is “convected”, i.e. distributed by CED, within the local extracellular fluid volume, it is expected to flow within both gray and white matter fractions. This is what was seen in our RCD MRI data. Although basal ganglia boundaries could be respected with cannula placement centered within the target nucleus, a more peripheral cannula placement allows for passage of GDL from within a gray matter structure into the adjacent white matter as described in this report. RCD with GDL also assists visualization of infusate reflux along the cannula tract and leakage of the CED infusate into the subarachnoid space or

[1]See FDA statement: http://www.fda.gov/bbs/topics/NEWS/2007/NEW01672.html

ventricular fluid, both of which could be potentially hazardous to the patient or limiting to the effective convection of the target volume.

In summary, we believe that RCD with GDL or other MR contrast agents may have an important role to play in the future of direct drug delivery to the CNS. In this study, we have noted a lack of acute toxicity with respect to clinical behavior and anatomically within the brain parenchyma of NHP's receiving multiple injections of GDL into various locations within the subcortical white and gray matter structures. We have demonstrated robust MR imaging capabilities of GDL with our RCD platform for drug delivery into corona radiata, putamen, and thalamus. There is a tight correlation between postoperative FMT-PET and AADC IHC. There is close correlation between convected GDL and AAV1 vectors within NHP brain. Since the AAV2 transfection is significantly less for white matter as opposed to gray matter, The correlation between GDL and AAV2 transfection is not as good as seen between GDL and AAV1 transfection. When GDL distribution in gray matter only is compared to AAV2 transfection volume, however, the correlation approaches that seen with GDL and AAV1. GDL is an accurate marker for AAV distribution and transfection within the NHP brain parenchyma, as long as one knows the relative affinity of the viral vector serotype used. While GDL distribution may correlate with intracellularly retained transgenes, such as AADC and GFP, further studies will be required to assess the imaging options for secreted transgene products, such as glial-derived neurotrophic factor (GDNF). A final word of caution is warranted; this is a relatively small study in an anatomically circumscribed region and although it appears that AAV1 correlates better with MRI-monitored delivery than does AAV2 this will need to be confirmed in a larger number of subjects.

Acknowledgments

These studies were supported by grants from NIH-NINDS. We would like to thank Drs. Shangzhen Zhou and Fraser Wright, Children's Hospital of Philadelphia, for the production of AAV2-hAADC.

References

Baekelandt V, De Strooper B, Nuttin B, Debyser Z. Gene therapeutic strategies for neurodegenerative diseases. Curr. Opin. Mol. Ther 2000;2:540–554. [PubMed: 11249757]

Bankiewicz KS, Oldfield EH, Chiueh CC, Doppman JL, Jacobowitz DM, Kopin IJ. Hemiparkinsonism in monkeys after unilateral internal carotid artery infusion of 1-methyl-4-phenyl-1,2,3,6-tetrahydropyridine (MPTP). Life Sci 1986;39:7–16. [PubMed: 3487691]

Bankiewicz KS, Eberling JL, Kohutnicka M, Jagust W, Pivirotto P, Bringas J, Cunningham J, Budinger TF, Harvey-White J. Convection-enhanced delivery of AAV vector in parkinsonian monkeys; in vivo detection of gene expression and restoration of dopaminergic function using pro-drug approach. Exp. Neurol 2000;164:2–14. [PubMed: 10877910]

Bankiewicz KS, Forsayeth J, Eberling JL, Sanchez-Pernaute R, Pivirotto P, Bringas J, Herscovitch P, Carson RE, Eckelman W, Reutter B, Cunningham J. Long-Term Clinical Improvement in MPTP-Lesioned Primates after Gene Therapy with AAV-hAADC. Mol. Ther 2006;14:564–570. [PubMed: 16829205]

Bobo RH, Laske DW, Akbasak A, Morrison PF, Dedrick RL, Oldfield EH. Convection-enhanced delivery of macromolecules in the brain. Proc. Natl. Acad. Sci. U. S. A 1994;91:2076–2080. [PubMed: 8134351]

Carter BJ. Adeno-associated virus vectors in clinical trials. Hum. Gene. Ther 2005;16:541–550. [PubMed: 15916479]

Chen MY, Lonser RR, Morrison PF, Governale LS, Oldfield EH. Variables affecting convection-enhanced delivery to the striatum: a systematic examination of rate of infusion, cannula size, infusate concentration, and tissue-cannula sealing time. J. Neurosurg 1999;90:315–320. [PubMed: 9950503]

Eberling JL, Jagust WJ, Christine CW, Starr P, Larson P, Bankiewicz KS, Aminoff MJ. Results from a phase I safety trial of hAADC gene therapy for Parkinson's disease. Neurology 2008;70:1980–1983. [PubMed: 18401019]

Fiandaca M, Forsayeth J, Bankiewicz K. Current status of gene therapy trials for Parkinson's disease. Exp. Neurol 2008;209:51–57. [PubMed: 17920059]

Forsayeth JR, Eberling JL, Sanftner LM, Zhen Z, Pivirotto P, Bringas J, Cunningham J, Bankiewicz KS. A dose-ranging study of AAV-hAADC therapy in Parkinsonian monkeys. Mol. Ther 2006;14:571–577. [PubMed: 16781894]

Gao G, Lu Y, Calcedo R, Grant RL, Bell P, Wang L, Figueredo J, Lock M, Wilson JM. Biology of AAV serotype vectors in liver-directed gene transfer to nonhuman primates. Mol. Ther 2006;13:77–87. [PubMed: 16219492]

Grieger JC, Samulski RJ. Adeno-associated virus as a gene therapy vector: vector development, production and clinical applications. Adv. Biochem. Eng. Biotechnol 2005;99:119–145. [PubMed: 16568890]

Grimm D, Kay MA. From virus evolution to vector revolution: use of naturally occurring serotypes of adeno-associated virus (AAV) as novel vectors for human gene therapy. Curr. Gene Ther 2003;3:281–304. [PubMed: 12871018]

Hadaczek P, Kohutnicka M, Krauze MT, Bringas J, Pivirotto P, Cunningham J, Bankiewicz K. Convection-enhanced delivery of adeno-associated virus type 2 (AAV2) into the striatum and transport of AAV2 within monkey brain. Hum. Gene Ther 2006A;17:291–302. [PubMed: 16544978]

Hadaczek P, Yamashita Y, Mirek H, Tamas L, Bohn MC, Noble C, Park JW, Bankiewicz K. The “perivascular pump” driven by arterial pulsation is a powerful mechanism for the distribution of therapeutic molecules within the brain. Mol. Ther 2006b;14:69–78. [PubMed: 16650807]

Hamilton JF, Morrison PF, Chen MY, Harvey-White J, Pernaute RS, Phillips H, Oldfield E, Bankiewicz KS. Heparin coinfusion during convection-enhanced delivery (CED) increases the distribution of the glial-derived neurotrophic factor (GDNF) ligand family in rat striatum and enhances the pharmacological activity of neurturin. Exp. Neurol 2001;168:155–161. [PubMed: 11170730]

Krauze MT, McKnight TR, Yamashita Y, Bringas J, Noble CO, Saito R, Geletneky K, Forsayeth J, Berger MS, Jackson P, Park JW, Bankiewicz KS. Real-time visualization and characterization of liposomal delivery into the monkey brain by magnetic resonance imaging. Brain Res. Brain Res. Protoc 2005a; 16:20–26. [PubMed: 16181805]

Krauze MT, Saito R, Noble C, Tamas M, Bringas J, Park JW, Berger MS, Bankiewicz K. Reflux-free cannula for convection-enhanced high-speed delivery of therapeutic agents. J. Neurosurg 2005b; 103:923–929. [PubMed: 16304999]

Krauze MT, Forsayeth J, Park JW, Bankiewicz KS. Real-time imaging and quantification of brain delivery of liposomes. Pharm. Res 2006;23:2493–2504. [PubMed: 16972184]

Krauze MT, Vandenberg SR, Yamashita Y, Saito R, Forsayeth J, Noble C, Park J, Bankiewicz KS. Safety of real-time convection-enhanced delivery of liposomes to primate brain: a long-term retrospective. Exp. Neurol 2008;210:638–644. [PubMed: 18295759]

Kunwar S, Prados MD, Chang SM, Berger MS, Lang FF, Piepmeier JM, Sampson JH, Ram Z, Gutin PH, Gibbons RD, Aldape KD, Croteau DJ, Sherman JW, Puri RK. Direct intracerebral delivery of cintredekin besudotox (IL13-PE38QQR) in recurrent malignant glioma: a report by the Cintredekin Besudotox Intraparenchymal Study Group. J. Clin. Oncol 2007;25:837–844. [PubMed: 17327604]

Lonser RR, Walbridge S, Garmestani K, Butman JA, Walters HA, Vortmeyer AO, Morrison PF, Brechbiel MW, Oldfield EH. Successful and safe perfusion of the primate brainstem: in vivo magnetic resonance imaging of macromolecular distribution during infusion. J. Neurosurg 2002;97:905–913. [PubMed: 12405380]

Lonser RR, Warren KE, Butman JA, Quezado Z, Robison RA, Walbridge S, Schiffman R, Merrill M, Walker ML, Park DM, Croteau D, Brady RO, Oldfield EH. Real-time image-guided direct convective perfusion of intrinsic brainstem lesions. Technical. note. J. Neurosurg 2007;107:190–197.

Mamot C, Drummond DC, Hong K, Kirpotin DB, Park JW. Liposome-based approaches to overcome anticancer drug resistance. Drug Resist. Updat 2003;6:271–279. [PubMed: 14643297]

Mamot C, Nguyen JB, Pourdehnad M, Hadaczek P, Saito R, Bringas JR, Drummond DC, Hong K, Kirpotin DB, McKnight T, Berger MS, Park JW, Bankiewicz KS. Extensive distribution of liposomes

in rodent brains and brain tumors following convection-enhanced delivery. J. Neurooncol 2004;68:1–9. [PubMed: 15174514]

Matsushita T, Elliger S, Elliger C, Podsakoff G, Villarreal L, Kurtzman GJ, Iwaki Y, Colosi P. Adeno-associated virus vectors can be efficiently produced without helper virus. Gene Ther 1998;5:938–945. [PubMed: 9813665]

Murad GJ, Walbridge S, Morrison PF, Szerlip N, Butman JA, Oldfield EH, Lonser RR. Image-guided convection-enhanced delivery of gemcitabine to the brainstem. J. Neurosurg 2007;106:351–356. [PubMed: 17410722]

Namavari M, Satyamurthy N, Phelps M, Barrio J. Synthesis of 6-[18F] and 4-[18F]Fluoro-l-meta-tyrosines via regioselective radiofluorodestannylation. Appl. Radiat. Isotopes 1993;44:527.

Neeves KB, Sawyer AJ, Foley CP, Saltzman WM, Olbricht WL. Dilation and degradation of the brain extracellular matrix enhances penetration of infused polymer nanoparticles. Brain Res 2007;1180:121–132. [PubMed: 17920047]

Nguyen JB, Sanchez-Pernaute R, Cunningham J, Bankiewicz KS. Convection-enhanced delivery of AAV-2 combined with heparin increases TK gene transfer in the rat brain. Neuroreport 2001;12:1961–1964. [PubMed: 11435930]

Paxinos, G.; Watson, C. The Rat Brain in Stereotaxic Coordinates. New York: Academic Press, Sydney; 1982.

Saito R, Bringas JR, McKnight TR, Wendland MF, Mamot C, Drummond DC, Kirpotin DB, Park JW, Berger MS, Bankiewicz KS. Distribution of liposomes into brain and rat brain tumor models by convection-enhanced delivery monitored with magnetic resonance imaging. Cancer Res 2004;64:2572–2579. [PubMed: 15059914]

Saito R, Krauze MT, Bringas JR, Noble C, McKnight TR, Jackson P, Wendland MF, Mamot C, Drummond DC, Kirpotin DB, Hong K, Berger MS, Park JW, Bankiewicz KS. Gadolinium-loaded liposomes allow for real-time magnetic resonance imaging of convection-enhanced delivery in the primate brain. Exp. Neurol 2005;196:381–389. [PubMed: 16197944]

Sampson JH, Brady ML, Petry NA, Croteau D, Friedman AH, Friedman HS, Wong T, Bigner DD, Pastan I, Puri RK, Pedain C. Intracerebral infusate distribution by convection-enhanced delivery in humans with malignant gliomas: descriptive effects of target anatomy and catheter positioning. Neurosurgery 2007;60ONS89-ONS98 discussion ONS98-89.

Samulski RJ, Berns KI, Tan M, Muzyczka N. Cloning of adeno-associated virus into pBR322: rescue of intact virus from the recombinant plasmid in human cells. Proc. Natl. Acad. Sci. U. S. A 1982;79:2077–2081. [PubMed: 6281795]

Sanchez-Pernaute R, Harvey-White J, Cunningham J, Bankiewicz KS. Functional effect of adeno-associated virus mediated gene transfer of aromatic L-amino acid decarboxylase into the striatum of 6-OHDA-lesioned rats. Mol. Ther 2001;4:324–330. [PubMed: 11592835]

Sanftner LM, Sommer JM, Suzuki BM, Smith PH, Vijay S, Vargas JA, Forsayeth JR, Cunningham J, Bankiewicz KS, Kao H, Bernal J, Pierce GF, Johnson KW. AAV2-mediated gene delivery to monkey putamen: evaluation of an infusion device and delivery parameters. Exp. Neurol 2005;194:476–483. [PubMed: 16022872]

Stefanini M, De Martino C, Zamboni L. Fixation of ejaculated spermatozoa for electron microscopy. Nature 1967;216:173–174. [PubMed: 4862079]

Sykova E. Extrasynaptic volume transmission and diffusion parameters of the extracellular space. Neuroscience 2004;129:861–876. [PubMed: 15561404]

Szerlip NJ, Walbridge S, Yang L, Morrison PF, Degen JW, Jarrell ST, Kouri J, Kerr PB, Kotin R, Oldfield EH, Lonser RR. Real-time imaging of convection-enhanced delivery of viruses and virus-sized particles. J. Neurosurg 2007;107:560–567. [PubMed: 17886556]

Urabe M, Ding C, Kotin RM. Insect cells as a factory to produce adeno-associated virus type 2 vectors. Hum. Gene Ther 2002;13:1935–1943. [PubMed: 12427305]

Varenika V, Dickenson P, Bringas J, LeCouteur R, Higgins R, Park JW, Fiandaca MS, Berger MS, Sampson JH, Bankiewicz KS. Real-time imaging of CED in the brain permits detection of infusate leakage. J. Neurosurg 2008;109:874–880. [PubMed: 18976077]

Vite CH, Passini MA, Haskins ME, Wolfe JH. Adeno-associated virus vector-mediated transduction in the cat brain. Gene Ther 2003;10:1874–1881. [PubMed: 14502216]

Wright JF, Qu G, Tang C, Sommer JM. Recombinant adeno-associated virus: formulation challenges and strategies for a gene therapy vector. Curr. Opin. Drug Discov. Dev 2003;6:174–178.

Wu Z, Asokan A, Samulski RJ. Adeno-associated virus serotypes: vector toolkit for human gene therapy. Mol. Ther 2006;14:316–327. [PubMed: 16824801]

Yin D, Valles FE, Fiandaca MS, Forsayeth J, Larson P, Starr P, Bankiewicz KS. Striatal Volume Differences Between Non-human and Human Primates. J. Neurosci. Methods. in press.

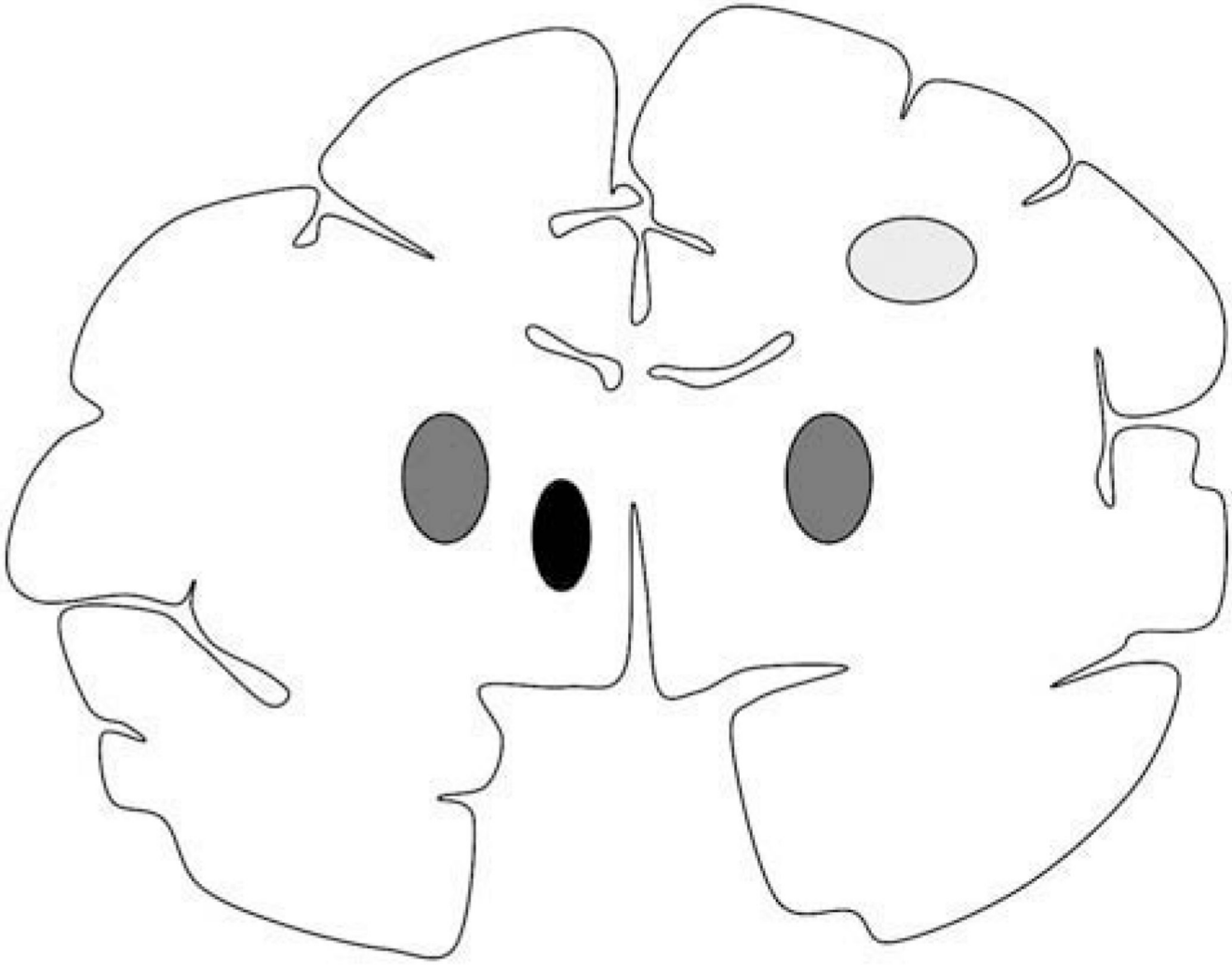

Fig. 1.

Schematic representation of the non-human primate brain in coronal section and sites of infusion. Region of corona radiata infused (light gray oval) in the right hemisphere in all three animals (NHP1, NHP2, and NHP3). Bilateral putaminal convections (dark gray ovals) were present in two NHP, whereas the remaining animal had only putaminal infusion in the right hemisphere. All three animals received thalamic infusion (black oval) in the left hemisphere.

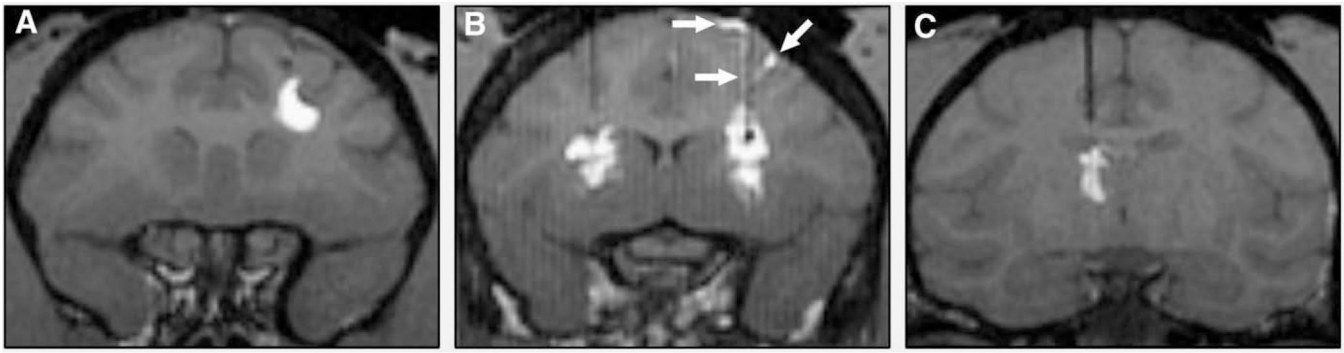

Fig. 2.
T1-weighted MR images of NHP RCD with GDL tracer. (A) Corona radiata. (B) bilateral putamen. (C) Thalamus. GDL contrast leak/reflux into subarachnoid space and along cannula tract (white arrows) is demonstrated in panel B.

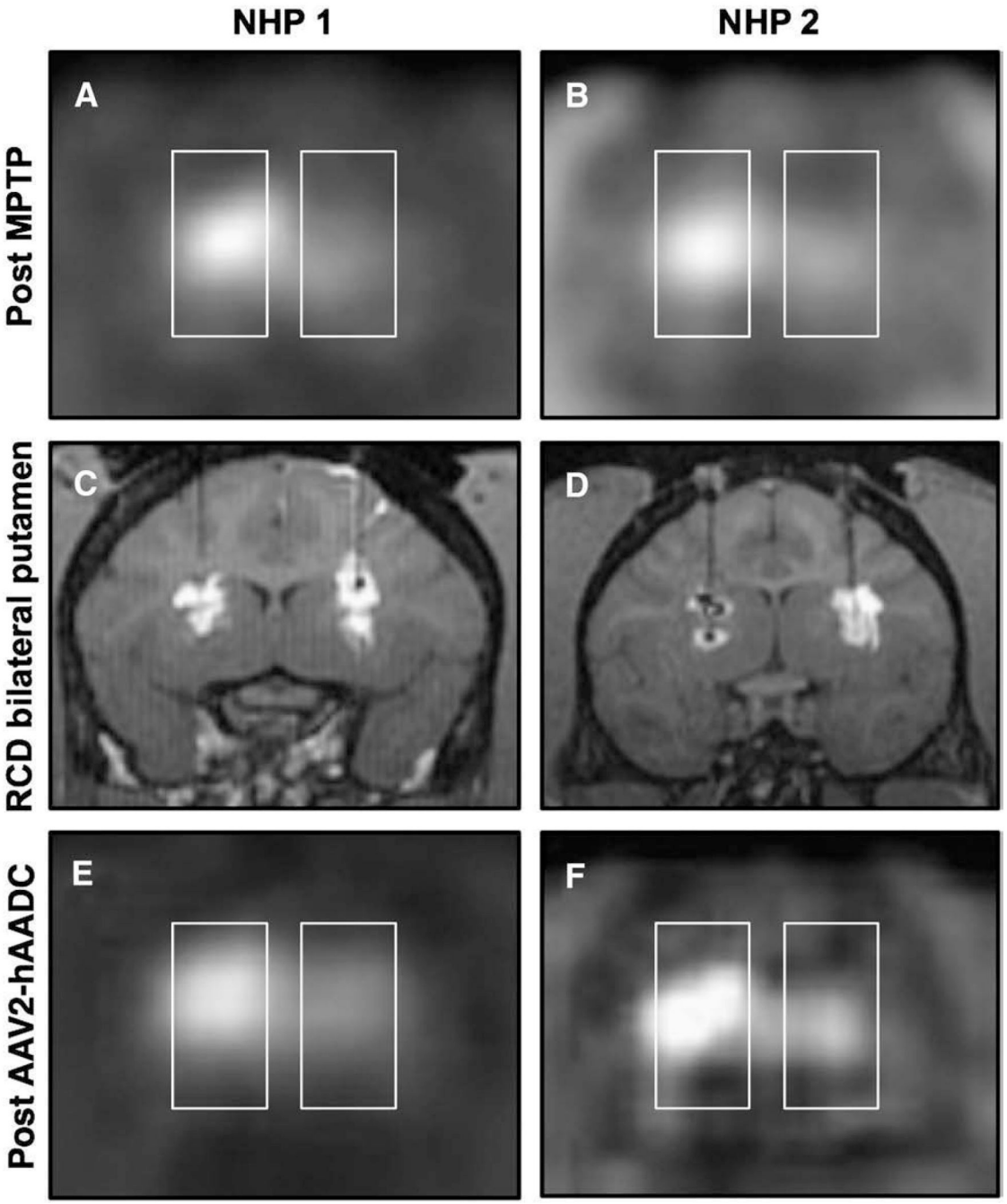

Fig. 3.

Coronal FMT-PET images after intracarotid MPTP. Panels A and B show a clear reduction in PET signal on the side ipsilateral to the intracarotid infusion. Bilateral RCD of putaminal targets (C and D) reveal robust bilateral GDL distribution in one subject (C), and MRI evidence of oil/air along with convection within the left putamen and otherwise robust convection within the right putamen of the other subject (D). Repeat FMT-PET after AAV2-hAADC gene therapy (E and F) shows a mild increase in bilateral PET signal in one subject (E), and marked increase in bilateral PET signal in the other animal (F).

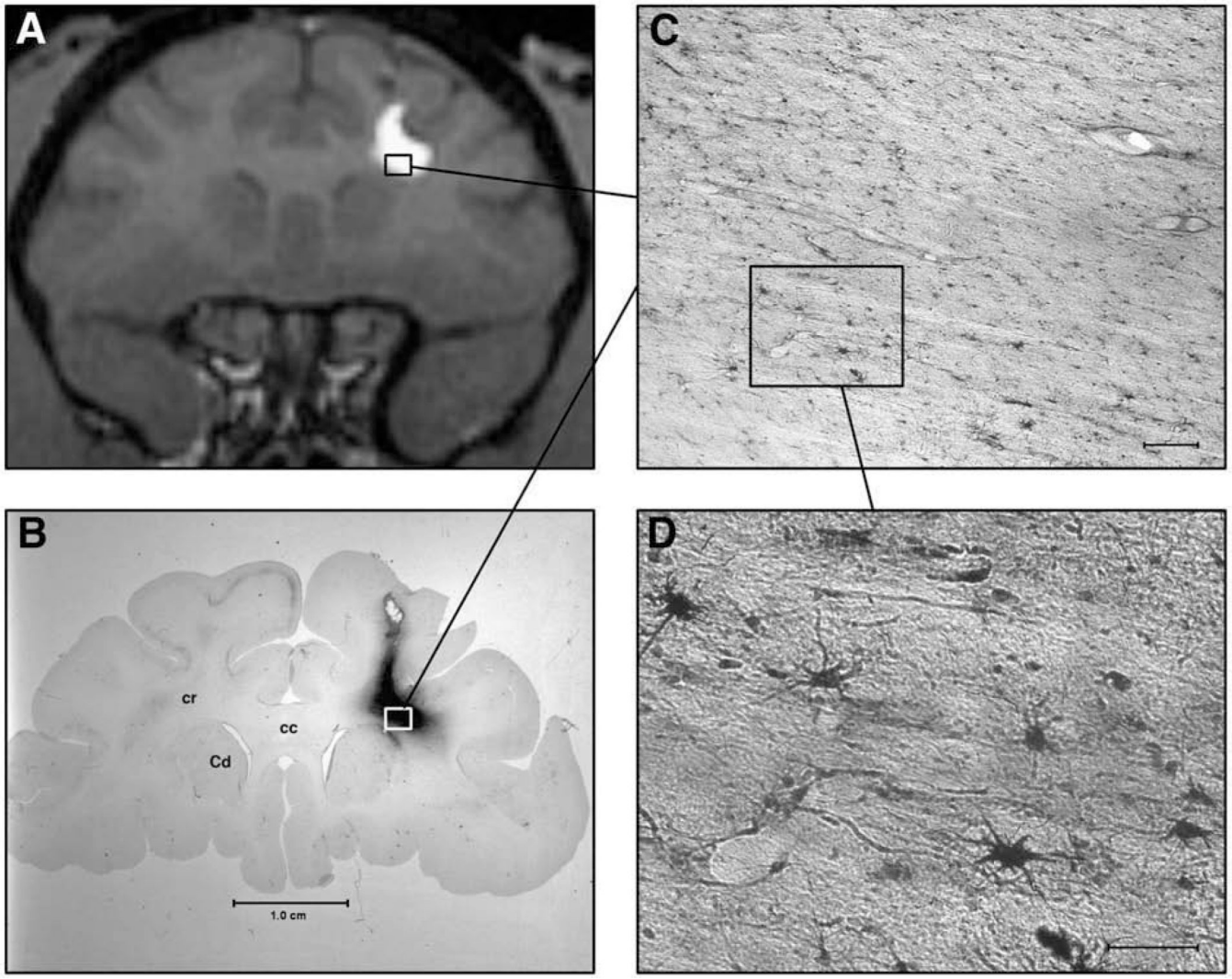

Fig. 4.

MRI correlation with histology in NHP with right corona radiata AAV1-GFP RCD. (A) T1-weighted coronal MR image of NHP brain with right corona radiata convection. GDL extends within the white matter tracts and, on this image, does not enter the adjacent head of caudate or overlying cortex. No leakage is noted in the subarachnoid space. (B) Histologic coronal brain section of animal depicted in A, showing GFP staining within the corona radiata (cr), with sparing of the corpus callosum (cc), overlying cortex, and adjacent head of caudate (Cd). (C) Low magnification view of specific GFP staining in the convected corona radiata. White matter tracts are easily seen, interspersed with positively stained nuclei. Scale-bar=0.25 mm. (D) High magnification view of boxed inset in C, showing positively stained astrocytic and oligodendrocytic nuclei. Scale-bar=0.10 mm.

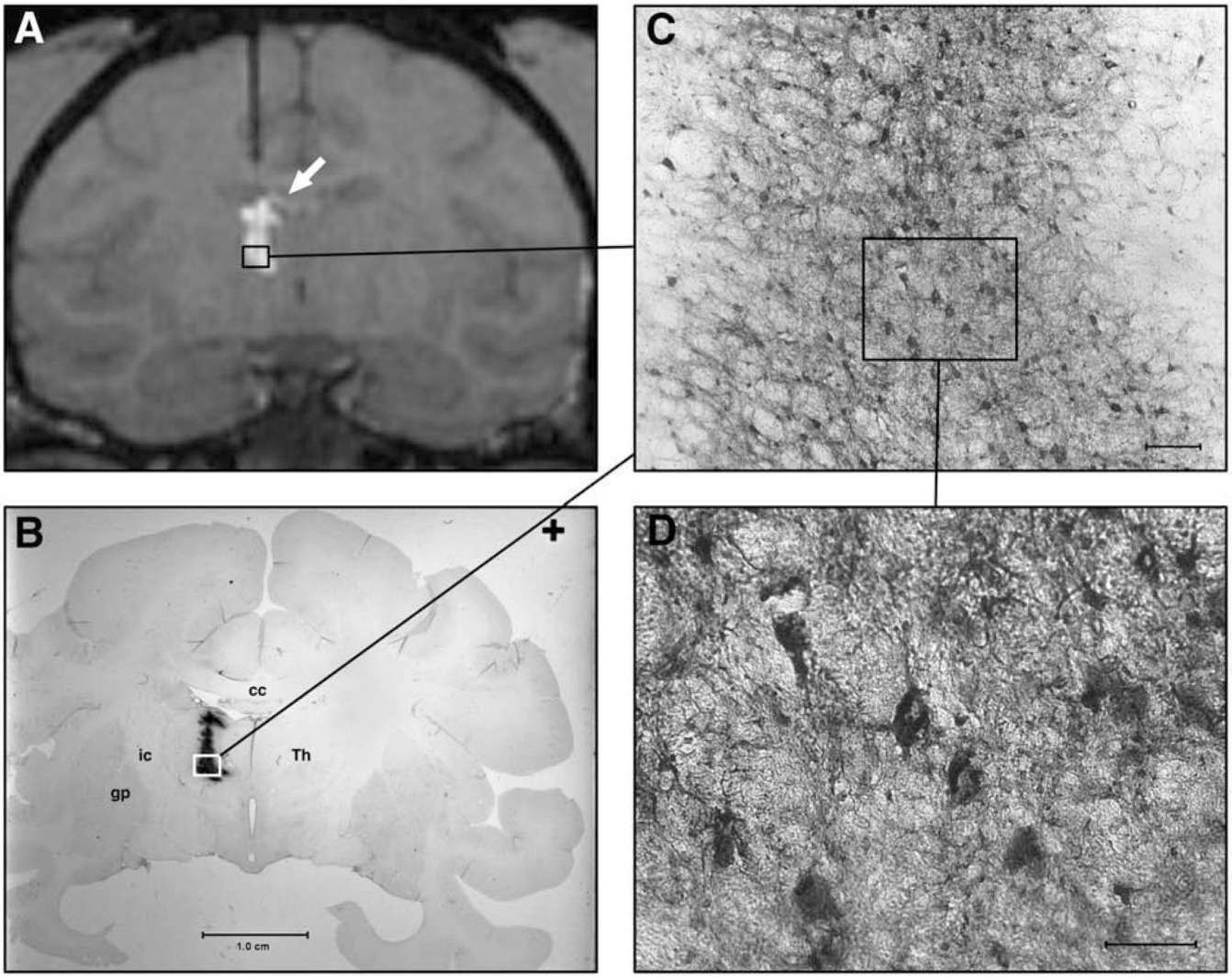

Fig. 5.

MRI correlation with histology in NHP with left thalamic AAV1-GFP RCD. (A) T1-weighted MR image showing cannula tract extending into left thalamus. Incomplete filling within the thalamus is noted as well as small amount of GDL leakage within the lateral ventricle (white arrow). (B) Coronal histologic section of NHP brain imaged in A, showing GFP in a pattern similar to that noted on MRI with GDL. Abbreviations: Thalamus (Th); globus pallidus (gp). (C) Low magnification view of thalamic region near cannula tip. Scale-bar=0.25 mm. (D) High magnification of boxed inset in C, showing GFP-positive cells within the thalamus. Both neurons and astrocytes are noted to be specifically stained. Scale-bar=0.10 mm.

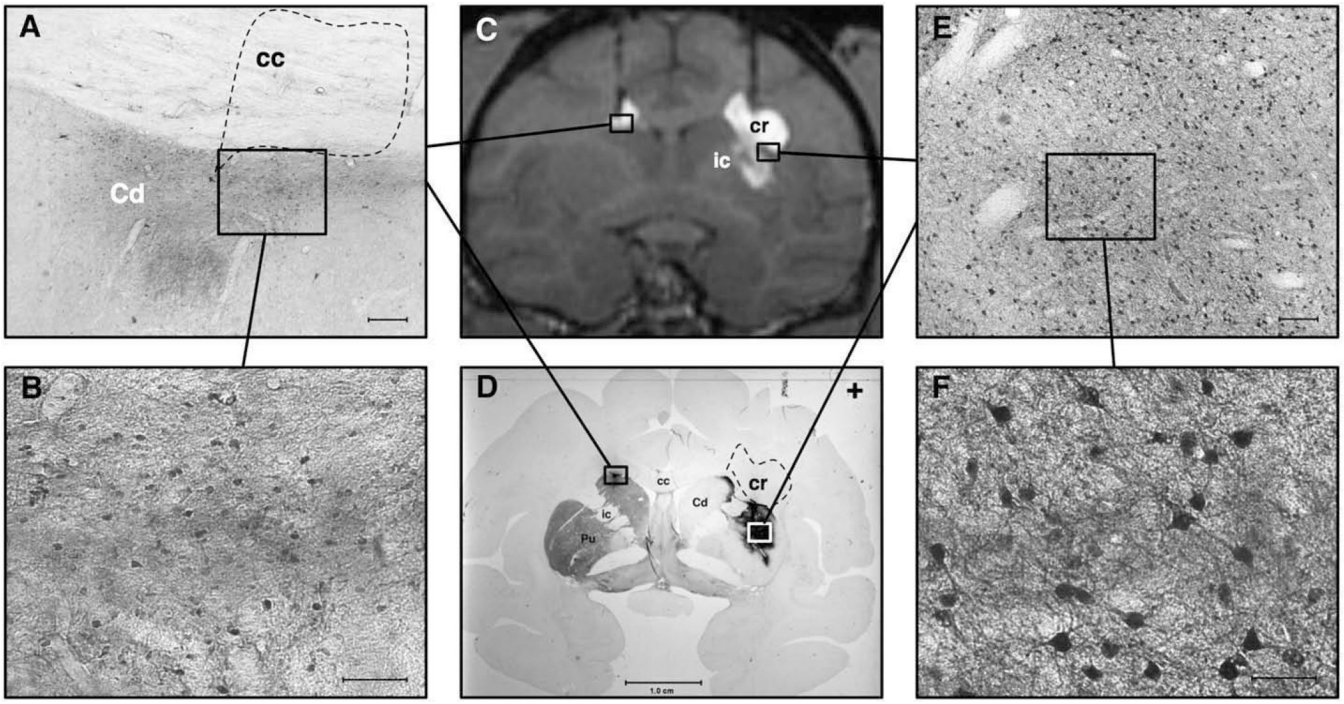

Fig. 6.

MRI correlation with histology in NHP with bilateral attempted putaminal AAV2-hAADC RCD. Panel A shows a low magnification view of the dorsolateral left head of the caudate (Cd) and overlying corpus callosum (cc). AADC staining is seen within the Cd after a medially placed cannula tract allowed it to be infused into this region rather than the left putamen. Notice the lack of specific AADC staining in the overlying corpus callosum (dotted polygon), despite GDL signal in this region on MRI (see C). Scale-bar=0.25 mm. Panel B depicts a representative view of higher magnification AADC staining in the left head of caudate. No such cellular staining was noted in the overlying white matter tracts. Scale-bar=0.10 mm. Panel C displays a coronal T1-weighted MR image of NHP brain with the bilateral RCD with GDL contrast. Although the putaminal targeting was better in the right hemisphere, there was some spread of the GDL into the internal capsule (ic) and overlying corona radiata (cr). The left-sided targeting was too medial and allowed convection of the head of the caudate and the overlying corpus callosum. Panel D shows a coronal histologic brain section of the same animal as imaged in panel C. This section is double-labeled, showing TH immunoreactivity (TH-IR) within the left striatum and paucity of TH-IR on the right, as a result of the right intracarotid MPTP infusion. The dense immunoreactivity in the left head of the caudate represents AADC IHC staining. Similar but more abundant AADC staining is seen within the substance of the right putamen, and part of the head of the right caudate. Note the absence of AADC staining within the overlying right corona radiata (dashed polygon, cr) and internal capsule, despite both of these regions showing GDL enhancement in panel C. Panel E depicts a low magnification view of the boxed region within the right putamen shown in D. Note the specific neuronal staining for AADC. Scale-bar=0.25 mm. Panel F shows a higher magnification view of the boxed region depicted within E. Notice the specific staining of medium spiny neurons. Scale-bar=0.10 mm.

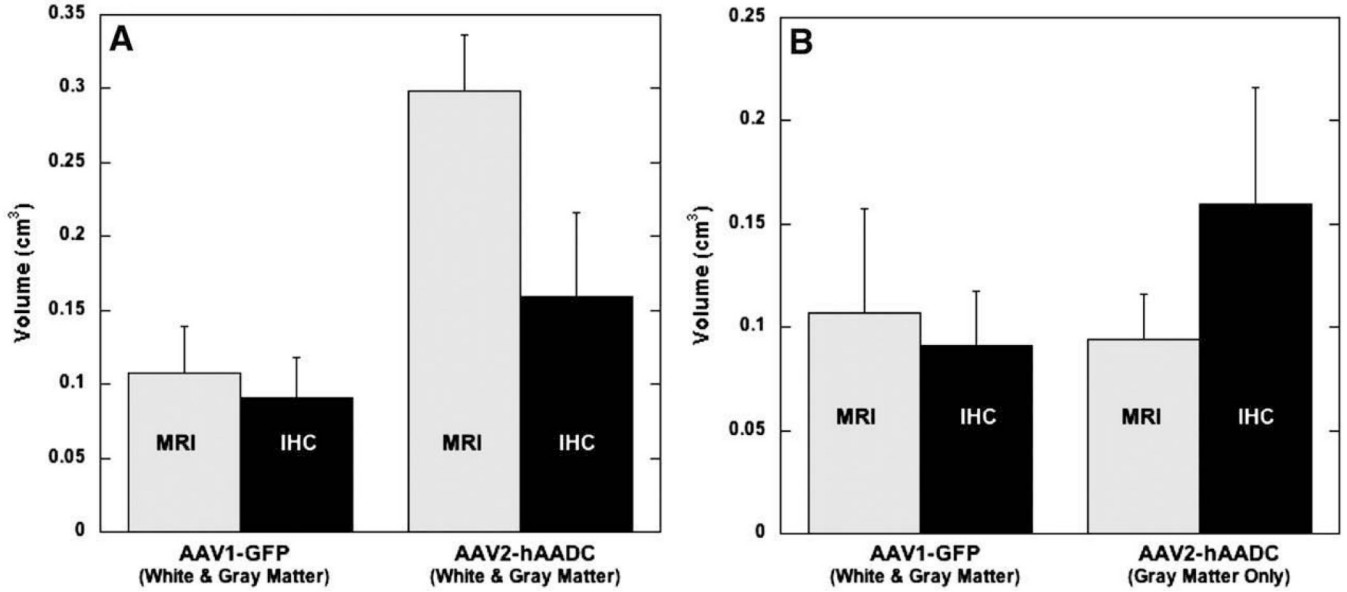

Fig. 7.

Vd differences between GDL, as noted on MR imaging, and specific IHC staining (for either GFP or AADC) in histologic brain sections. (A) Comparison of mean Vd of GDL, Vd of GFP (AAV1-GFP) and Vd of AADC (AAV2-hAADC) in both gray and white matter. (B) Keeping the same GDL and GFP IHC (AAV1-GFP) mean Vd comparison, we plotted the GDL mean Vd and AADC IHC (AAV2-hAADC) mean Vd in gray matter only. Error bars show SEM.